ACS APPLIED MATERIALS & INTERFACES

www.acsami.org

Research Article

Molecular Dynamics Study of the Thermodynamics of Integer Charge Transfer vs Charge-Transfer Complex Formation in Doped Conjugated Polymers

Eric Chih-Kuan Wu, Charlene Z. Salamat, Sarah H. Tolbert, and Benjamin J. Schwartz*

Cite This: *ACS Appl. Mater. Interfaces* 2022, 14, 26988–27001

Read Online

ACCESS | Metrics & More | Article Recommendations | Supporting Information

ABSTRACT: Molecular dopants such as 2,3,5,6-tetrafluoro-7,7,8,8-tetracyanoquinodimethane (F_4TCNQ) can interact with conjugated polymers such as poly(3-hexylthiophene-2,5-diyl) (P3HT) in two different ways: they can undergo integer charge transfer (ICT) or they can form a partial-charge-transfer complex (CTC). Both are seen experimentally, but the CTC has been challenging to characterize, making it difficult to answer questions such as the following. Which polymorph is more stable? Do they have similar barriers for formation? Is there a thermodynamic route to convert one to the other? Here, we study the structure and the thermodynamics of bulk F_4TCNQ-doped P3HT with all-atom molecular dynamics simulations, using thermodynamic integration to calculate the relative free energies. We find that the ICT and CTC polymorphs have similar thermodynamic stabilities. The barrier to create the ICT polymorph, however, is lower than that to make the CTC polymorph, because the ICT polymorph has a small critical nucleus, but the critical nucleus for the CTC polymorph is larger than what we can simulate. Moreover, simulated thermal annealing shows that the activation barrier for converting the CTC polymorph to the ICT polymorph is relatively modest. Overall, the simulations explain both the observed structures and the thermodynamics of F_4TCNQ-doped P3HT and offer guidelines for targeting the production of a desired polymorph for different applications.

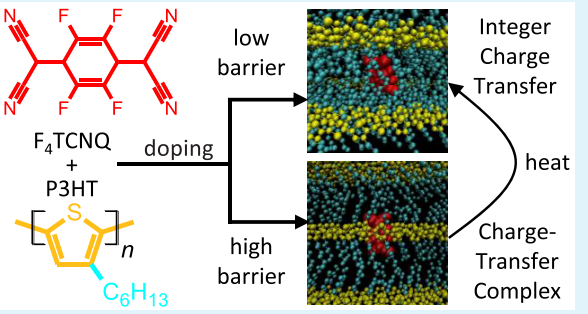

KEYWORDS: *semiconducting polymers, molecular dopants, integer charge transfer, charge-transfer complex, thermodynamics vs kinetics*

1. INTRODUCTION

Conjugated organic semiconductors offer great promise as the active materials for applications in flexible electronics, including light-emitting diodes, photovoltaics, and thermoelectric devices.[1−5] For many of these applications, organic semiconductors need to be doped by adding charge carriers, i.e., holes or electrons, into the π-systems of these materials. This can be accomplished through either electrochemical or chemical doping. In chemical doping, a strong oxidizing (or reducing) agent is added to inject holes (or electrons) into the conjugated π-system. Most organic semiconductors are p-type materials; thus, they are doped by adding strong oxidizing agents to remove electrons from the π-conjugated backbone.

In general, molecular dopants have two ways to interact with organic semiconductors. One way is that the dopants and the organic semiconductors share their molecular orbitals, allowing for partial charge transfer between them and thus the formation of charge-transfer complexes (CTCs).[6,7] This is the preferred mode of interaction in charge-transfer salts, which are cocrystals of small-molecule organic donors and acceptors. Alternatively, for materials such as conjugated polymers, dopant molecules almost always reside in the lamellar region of the polymer crystallites, among the side chains that are much farther from the π-system on the polymer backbone.[6,8−10] In this situation, the wave functions of the conjugated polymer π-system and the dopant do not overlap, and the result is transfer of a full electron from the conjugated polymer to the dopant acceptor, or integer charge transfer (ICT).

In the doped conjugated polymer literature, ICT appears to dominate following molecular doping, and CTC formation, involving a polymorph where the dopants π-stack with the polymer backbone, is relatively rare.[11−26] The fact that CTCs do not readily form in doped conjugated polymers is generally desirable since CTCs are not associated with the production of mobile charge carriers needed for various device applications. In fact, one has to go to great lengths to produce significant amounts of the CTC polymorph in doped semiconducting

Received: April 12, 2022
Accepted: May 6, 2022
Published: June 3, 2022

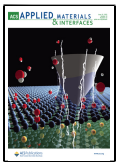

polymer films, using extreme processing conditions such as heating the solutions during film deposition[26] or using specially designed conjugated polymers with branched side chains that block dopants from occupying the lamellar region.[12]

Recently, we systematically investigated the doping of the well-studied conjugated polymer poly(3-hexylthiophene-2,5-diyl) (P3HT; Figure 1f) with the commonly used strong oxidizing agent 2,3,5,6-tetrafluoro-7,7,8,8-tetracyanoquinodimethane (F_4TCNQ, Figure 1e).[27] We showed that CTCs and ICT are both always present in doped semiconducting polymer films and that the relative amount of CTCs formed upon doping can be controlled by the dopant infiltration conditions. If the P3HT film is cast first, we found that the use of chloroform as a solvent to infiltrate the dopant leads to one order of magnitude more CTC formation in comparison to the use of dichloromethane (DCM). This is because chloroform partially dissolves the underlying polymer film and allows for recrystallization into the CTC π-stacked polymorph, whereas DCM only swells the polymer and does not dissolve it, leaving the original polymer crystallites largely intact.[27] We also demonstrated that introducing the F_4TCNQ dopant from the vapor phase creates fewer CTCs in comparison to infiltrating the dopants from solution and that doping P3HT films that start with higher crystallinity from either the vapor or solution phases results in less CTC formation. Finally, we also argued that ICT is thermodynamically favored, because annealing doped P3HT films with a large fraction of CTCs at only 80 °C for 5 min was enough to convert most of the CTC polymorph to the ICT polymorph.[27]

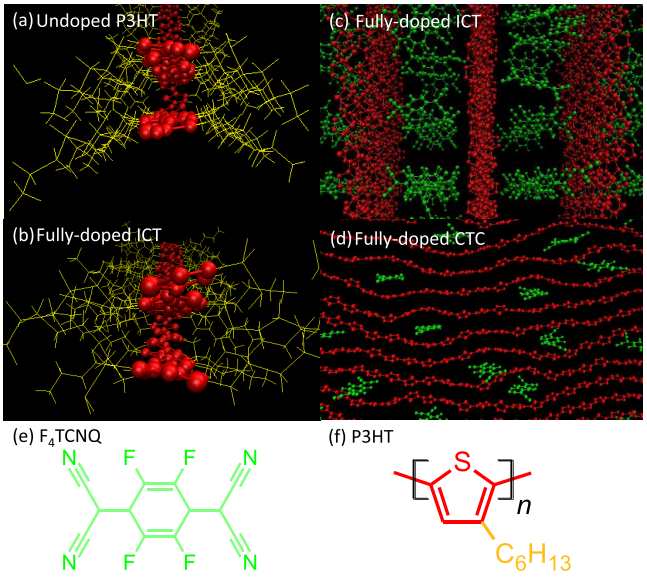

Figure 1. Simulation snapshots of (a) undoped P3HT, (b, c) the fully F_4TCNQ-doped ICT polymorph, and (d) the fully F_4TCNQ doped CTC polymorph. Only a small fraction of the P3HT chains in each snapshot are shown for clarity. For (c) and (d), the P3HT hexyl chains are not shown. (a) and (b) show the view down the polymer backbone (unit cell *c* axis), with the unit cell *b* axis running vertically. (c) shows a top view of the polymer backbone (looking down the unit cell *b* axis with the *c* axis running vertically). (d) shows the view looking down the hexyl chains (unit cell *a* axis), with the unit cell *b* axis running vertically. The atoms and bonds highlighted in red are part of the polymer backbone, while those represented by yellow sticks are part of the hexyl side chains. The F_4TCNQ molecules in (c) and (d) are highlighted in green; the F_4TCNQ dopants are not shown in (b) for clarity. (e) and (f) show the chemical structures of F_4TCNQ and P3HT, respectively.

For all of this experimental work, however, there are still many questions left unanswered concerning the formation kinetics and relative thermodynamic stabilities of the CTC and ICT polymorphs in doped conjugated polymer films. These questions include the following. What is the free energy cost for producing the ICT polymorph with the dopant in the polymer lamellae versus creating the CTC polymorph with the polymer and dopant in a π-stacked arrangement? Does the free energy for producing a doped polymorph depend on the number of dopants in the system (i.e., are there nucleation effects for producing either the ICT or CTC polymorphs)? What is the barrier for converting the CTC phase to the more desirable ICT phase and vice versa? In this paper, we use all-atom molecular dynamics (MD) simulations to provide qualitative thermodynamic answers to these questions by studying the structures of pristine P3HT and the CTC and ICT polymorphs of P3HT doped with F_4TCNQ, the thermodynamics of the doping process, and the kinetics of interconverting between the different doped polymorphs. Our simulation cell consists of 6 stacks of 12 P3HT chains (for a total of 72 chains) that each have 24 thiophene monomer units (1728 monomers in total), along with various numbers of F_4TCNQ molecules in different doping geometries, which with periodic boundary conditions in all three directions provides a reasonable approximation to the bulk material. We note that, although there have been many computational studies examining the doping of conjugated polymers, most either looked only at single oligomers and dopant molecules in the gas phase[28−34] or examined the structure and mechanical properties of the pure P3HT polymer without including dopant molecules.[35−48] As far as we know, this represents the first work using simulation methods to study the bulk structure with dopant molecules and the thermodynamics of the doping process for semiconducting polymers.

It is worth noting that, by using classical MD simulations, we are implicitly making assumptions that integrate out quantum mechanical degrees of freedom that might be important in determining the thermodynamics of the conjugated polymer doping process. We chose classical MD because understanding thermodynamics requires the simulation of systems that are large enough such that any quantum mechanical treatment, even with methods such as density functional theory (DFT), are far out of computational reach. As we will show below, however, our classical simulations are able to reproduce experimental X-ray-determined structure factors for undoped P3HT and both the CTC- and ICT-doped polymorphs. The simulations also successfully predict the conversion of the CTC polymorph to the ICT polymorph upon modest thermal annealing that is observed experimentally.[29] To ensure that the conclusions we draw are robust, we also performed simulations with several different force fields and found that the thermodynamics did not qualitatively change. This suggests that, despite being classical approximations to a quantum mechanical system, our simulations are useful for obtaining thermodynamic insights and can provide guidelines for designing materials to favor one or the other polymorph for different applications.

The rest of this paper is organized as follows. In Section 2.1, we introduce one of the force fields that we used to calculate the structure of undoped P3HT films, providing a direct means to validate our simulations against experimental X-ray

https://doi.org/10.1021/acsami.2c06449
ACS Appl. Mater. Interfaces 2022, 14, 26988−27001

diffraction experiments. We find that the simulated structure is in excellent qualitative agreement with experimental diffraction patterns. We then insert different numbers of F_4TCNQ dopants into the system in different locations to simulate the CTC- and ICT-doped polymorphs and then use the simulation results to examine the changes in structure upon doping. In Section 2.2, we use thermodynamic integration to calculate the free energy, enthalpy, and entropy associated with the different polymorphs of F_4TCNQ-doped P3HT. The results indicate that the free energy barrier to create the ICT polymorph is lower than that to create the CTC polymorph. This is because creation of the ICT polymorph shows a critical nucleus size of only 2−3 dopant molecules, after which there is effectively no penalty for expanding the ICT phase. In contrast, we were unable to observe nucleation effects for creating the CTC phase, suggesting either a very large critical nucleus for CTC phase formation or possibly a complete lack of nucleation effects for this phase. We also see that the ICT and CTC polymorphs have similar overall thermodynamic stabilities at room temperature, but the fact that they have different doping entropies means that their relative stabilities are highly sensitive to temperature. In Section 2.3, we simulate thermal annealing of F_4TCNQ-doped P3HT in the CTC polymorph and find that the barrier for converting the CTC to the ICT polymorph is only ∼140 meV, in qualitative agreement with the experimental observation that modest heating can convert the CTC polymorph to the ICT polymorph. We summarize the results in Section 3, and our simulation methodology is described in Section 4. The force field parameters and the results from several other force fields to show that our conclusions are qualitatively robust are detailed in the Supporting Information. Overall, our MD simulations are able to paint a qualitatively accurate picture of the doping process in conjugated polymer films. The results explain why CTCs are always present in doped polymer films even though the ICT state is kinetically preferred and offer guidelines for enhancing or avoiding a particular polymorph for the desired applications.

2. RESULTS AND DISCUSSION

2.1. Methodology for Simulating the Doping of Bulk P3HT Films with F_4TCNQ. We begin our exploration of the simulated properties of doped and undoped P3HT films by introducing one of the force fields used in this study, which is a derivative of the OPLS-AA force field.[49] This force field was developed by Wildman et al.,[50] who performed a dihedral angle scan along the P3HT backbone using CAM-B3LYP/6-31G* to optimize the molecular geometry and CAM-B3LYP/cc-pVTZ to calculate single-point energies. These workers then modified the OPLS-AA force field parameters so that the potential energy along the dihedral angles of the polymer backbone matched the DFT results; the other OPLS-AA parameters were left unchanged. These workers showed that the force field reproduced experimental measurements of P3HT persistent lengths,[50] and this force field also has been used in another computational study of P3HT.[51] In the Supporting Information, we present a comparison of the results using this force field to those using two other force fields. All three force fields produce the same qualitative results, which suggest that the conclusions we draw from our simulations are qualitatively robust.

2.1.1. Simulating Bulk Undoped P3HT. Before examining the thermodynamics and structure of P3HT doped with F_4TCNQ, we first compare the simulated undoped structures with those of experimental X-ray and electron diffraction studies. As was mentioned above, our simulation box consists of 6 stacks of 12 P3HT chains (for a total of 72 chains) that each have 24 thiophene monomer units (1728 monomer units in total); with periodic boundary conditions along all three axes, this provides a reasonable approximation of the bulk material. The initial structures were generated using the Avogadro program's universal force field, a simple molecular mechanics force field.[52] For the initial structure, we did not take special care in stacking the P3HT chains and instead only ensured through the use of Avogadro that the bond lengths and angles were reasonably close to their optimal values. Then, using GROMACS,[53−56] we annealed the systems at 600 K and then at 500 and 400 K for 1 ns each, after which the systems were equilibrated at room temperature (300 K) for an additional 10 ns in the isobaric−isothermal ensemble (NPT), with the pressure chosen to achieve the experimental bulk density of 1.1 g/cm^3. Details of the simulations and force field parameters can be found in Section 4 and in the Supporting Information. During the 10 ns equilibration, the P3HT chains formed their bulk crystal structure spontaneously.

Figure 2a shows a comparison of the experimental and simulated structure factors, $S(q)$, for P3HT. Details of the experimental methods can be found in the Supporting Information. $S(q)$ is calculated using the built-in function of GROMACS, which uses a fast Fourier transform. As with most semicrystalline polymers, there are three principal features seen in the structure factors. The first is the (100) peak or a axis repeat distance, near 0.35 Å^{-1} (plus several overtones), which corresponds to the lamellar spacing between the P3HT backbones. The second peak is the (020) or b axis repeat distance, near 1.65 Å^{-1}, which corresponds to the (tilted) P3HT π-stack distance. The third feature is the (001) peak or c axis repeat distance, near 1.2 Å^{-1}, which corresponds to the distance between the thiophene rings along the polymer backbone. The (001) peak has a low intensity and appears near the (300) peak; thus, it is not distinct.

Figure 2a shows that the force field developed by Wildman et al.,[50] which was optimized specifically for P3HT, reproduces the correct experimental (020) distance. By looking directly down the polymer backbone (Figure 1a), we see that the simulation produces a P3HT crystal structure where the polymer π-stacking direction is orthogonal to the chain axis. Electron diffraction experiments have shown that the P3HT backbone is tilted by 26° with respect to the unit cell b axis, which is oriented vertically in Figure 1a, indicating that, even though the force field is reproducing the correct π-stacking distance, it is not capturing this aspect of the polymer structure.[57] For comparison, we also performed limited simulations using the unmodified OPLS-AA force field (orange curve in Figure 2a), which predicts an (020) π-stacking distance that is larger ($S(q)$ peak at smaller q) than that of the Wildman et al. force field. The ∼1.45 Å^{-1} (020) peak position predicted by OPLS-AA is more in accord with the disordered π-stacking seen experimentally in regiorandom P3HT and amorphous regioregular P3HT,[58,59] which suggests that the lack of optimization of the dihedral potentials produces a less-ordered, more-amorphous overall structure. Figure 2a also shows that the Wildman et al.[52] and OPLS-AA force fields both predict a (100) lamellar peak position that is in reasonable agreement with experiment.

https://doi.org/10.1021/acsami.2c06449
ACS Appl. Mater. Interfaces 2022, 14, 26988−27001

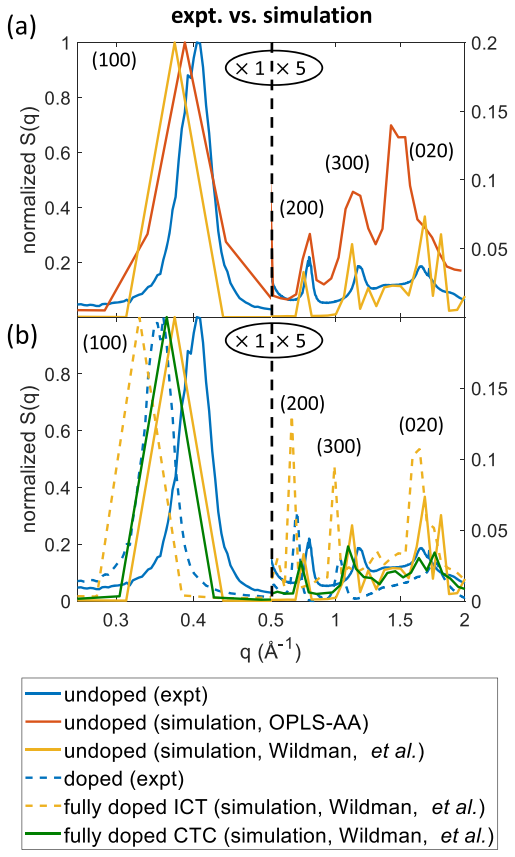

Figure 2. (a) Structure factors, $S(q)$, of undoped P3HT from experiments (blue) and from simulations with two different force fields: orange, OPLS-AA; yellow, Wildman et al.[50] (b) Experimental structure factors of undoped (blue) and doped (blue dashed line) P3HT and the calculated structure factors of undoped P3HT (yellow), fully F_4TCNQ doped P3HT with the F_4TCNQ dopants in the crystallite lamellae (yellow dashed line; ICT polymorph) and in the polymer π-stacks (green; CTC polymorph). All structure factors are normalized to the height of the (100) peak. For both panels, the horizontal axis scale changes at 0.5 Å^{-1}, as indicated by the vertical dashed line. To the right of the scale break, the y axis is expanded to better show the (h00) overtones and the (020) peak. For the experimental doped structure factors, the P3HT films were cast from o-dichlorobenzene and then sequentially doped with a 6 mg/mL solution of F_4TCNQ in n-butylacetate (see the Supporting Information). Results for other force fields, which are qualitiatively similar, are shown in the Supporting Information.

In the Supporting Information, we also simulate the P3HT structure with two additional force fields, both of which have stiffer torsional potentials in comparison to the Wildman et al. force field.[50] We find that both of these alternate force fields also produce similar structure factors and that one of them even partially captures the tilt of the thiophene backbone relative to the unit cell. The fact that multiple force fields yield similar results indicates that the P3HT unit cell structure is primarily determined by how the molecule fills space and that finer details of the interactions are of lesser importance, which is what allows us to use classical MD to draw structural and thermodynamic conclusions about this inherently quantum mechanical system.

2.1.2. Simulating Bulk P3HT with a Single F_4TNCQ Dopant. With force fields that are able to reproduce structural features that are in generally good agreement with experiment, we now turn to simulations of doping the polymers. There are two primary ways to insert a single F_4TCNQ molecule into a simulation of crystalline P3HT: the dopant can be inserted into the lamellar region of a P3HT crystallite to form the ICT state, or it can be placed into one of the P3HT π-stacks to form a CTC. To simulate a single ICT, we inserted an F_4TCNQ molecule into one of the lamellar regions of the simulated pure P3HT crystallites with the long axis of the dopant molecule being oriented parallel to the a axis of the P3HT unit cell. This orientation was chosen as the best match to what was determined experimentally for the ICT polymorph by Brinkmann and co-workers.[14,59]

In our simulations, the F_4TCNQ molecule carries a full negative charge at its molecular center. We elected to split the counterbalancing positive charge on the two neighboring P3HT chains across the lamellae. We made this choice because we found that if the polaron's positive charge were placed on a single chain, the F_4TCNQ molecule would push the polymer's hexyl side chains aside to be as close as possible to the charged polymer backbone. Experimentally, however, there is strong evidence that the dopant anion resides in the center of the lamellae, about 7−8 Å from the P3HT chains on either side,[14,33] and we found that splitting the positive charge between chains produced exactly this result. We distributed the positive 0.5e charge on each neighboring polymer chain in a Gaussian manner with a full width (2σ) of six monomer units, with the charge on each monomer unit distributed equally among the heavy atoms of each thiophene ring. We note that our laboratory recently measured the intrachain coherence length of polarons in doped crystalline P3HT using the vibrational Stark effect,[60] and we chose the size of the polaron in our calculations to match what we experimentally measured.

To simulate a single CTC, after preparing the simulation cell with pure crystalline P3HT, we inserted a single F_4TCNQ molecule between two of the P3HT π-stacked thiophene rings, a geometry that should be consistent with X-ray diffraction experiments that have studied the F_4TCNQ:P3HT CTC polymorph.[26,27] DFT calculations, which are described in more detail in the Supporting Information, suggest that a P3HT:F_4TCNQ CTC undergoes transfer of 0.59 of an electron between the two molecular species. Thus, to simulate a single CTC, we distributed a positive 0.59 charge across the thiophene rings centered on one of the P3HT chains that π-stacks with the dopant. The positive charge distribution was spread in a Gaussian fashion with a 2σ value of four monomer units in the same manner as for the ICT polymorph described above. Unlike the ICT polymorph, we placed the positive P3HT charges for the CTC polymorph on only a single chain. This is because we found that putting the positive charges on two neighboring P3HT π-stacked chains caused the two chains to repel each other and weakened the π-stack. For the −0.59e-charged F_4TCNQ counterion in the CTC, we used the Mulliken charges from the DFT calculations (see Table S6 in the Supporting Information).

It is worth noting that our simulations do not explicitly include the "benzoid-to-quinoid" conformational change along the P3HT backbone that takes place upon doping and polaron formation, which should affect the stiffness of the backbone dihedral angles relative to the neutral polymer. This is why one of the additional force fields we tested in the Supporting Information has a much stiffer P3HT backbone. We found, however, that the stiffer backbone produces essentially the same structure factor as the Wildman et al. force field discussed

https://doi.org/10.1021/acsami.2c06449
ACS Appl. Mater. Interfaces 2022, 14, 26988−27001

here.[50] This again suggests that the way the molecules fill space in the different polymorphs is more important than the details of their quantum mechanical interactions, giving us confidence in the conclusions we draw below.

2.1.3. Simulating Bulk P3HT with a Few F_4TNCQ Dopants. To study nucleation effects in transforming the pure P3HT system into one of its doped polymorphs, we also prepared simulations with more than a single dopant. For the ICT polymorph, we manually inserted two, three, or four F_4TCNQ molecules into the same lamellar stack of a P3HT crystallite with the long axis of the dopant molecule oriented parallel to the *a* axis of the P3HT unit cell. We chose different positions of the F_4TCNQ molecules relative to the thiophene rings, which are shown in Figure 3a–c. We label the four different relative dopant positions as "along-chain", "perp", "triangle", and "triangle (tight)". For both the "along-chain" and "perp" simulations, we placed the F_4TCNQ molecules in a straight line. Our "along-chain" simulations had the F_4TCNQ molecules inserted into the same lamellar stack but spaced six thiophene units apart along the P3HT backbone (red line in Figure 3a). For our "perp" simulations, we placed the line of inserted F_4TCNQ molecules perpendicular to the polymer backbone, i.e. parallel to the *b* axis of the P3HT unit cell, and we placed the F_4TCNQ molecules one P3HT chain apart (purple line in Figure 3a).

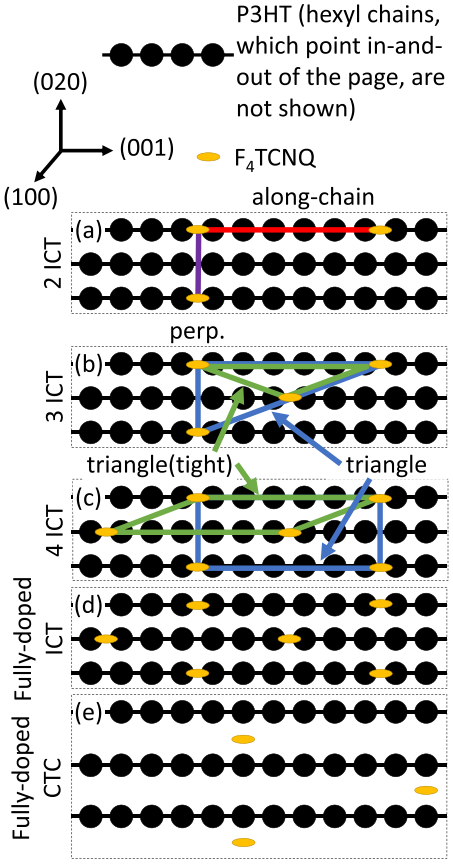

Figure 3. Relative positions of F_4TCNQ molecules chosen for (a) "2 ICT", (b) "3 ICT", (c) "4 ICT", (d) "fully doped ICT", and (e) "fully doped CTC". The cartoon shows the view down the P3HT unit cell *a* axis with the unit cell *b* axis running vertically. The black circles represent thiophene rings, and the yellow circles represent F_4TCNQ molecules. The hexyl chains (not shown for clarity) point in and out of the page. The F_4TCNQ molecules connected by the red line represent the "along-chain" orientation. The F_4TCNQ molecules connected by the purple line represent the "perp" orientation. The F_4TCNQ molecules connected by the blue lines represent the "triangle" orientation. The F_4TCNQ molecules connected by the green lines represent the "triangle (tight)" orientation. The polaronic charges on P3HT are not shown for simplicity. The "along-chain" and "perp" orientations are not shown for "3 ICT" and "4 ICT".

For the "triangle" and "triangle (tight)" simulations, we placed the F_4TCNQ molecules either along neighboring P3HT chains ("triangle (tight)") or spaced one P3HT chain apart ("triangle"). As an example of the different triangle geometries, for "3 ICT", we placed two F_4TCNQ molecules in the lamellar region along the same P3HT chain (chain 1) and one F_4TCNQ molecule in the same lamellar region but aligned along a different chain (chain 2). For "triangle (tight)", chains 1 and 2 are neighboring chains (green lines in Figure 3b); for "triangle", chains 1 and 2 have a P3HT chain in between (blue lines in Figure 3b). As with the single ICT simulations, the polarons (not shown in Figure 3) are split on the two neighboring P3HT chains across the lamellae, and the positive charges are distributed on each chain in a Gaussian manner with a 2σ value of six monomer units. When multiple polarons overlapped on the same P3HT chain, the total polaronic charge on each unit was added.

For the CTC-doped polymorph, we prepared a simulated system with two F_4TCNQ molecules inserted into the same P3HT π-stack. The two F_4TCNQ molecules in the CTC polymorph were initially placed six monomer units apart (Figure 4a), but as the system equilibrated, we saw that the two F_4TCNQ molecules diffused toward each other until they became adjacent (Figure 4b). When the two F_4TCNQ molecules are six monomers apart, the thiophene rings on the adjacent P3HT chains between the two dopants cannot make a good π-stack, so that the π-stacked space between the two F_4TCNQ molecules has a lower density. This creates a net force that drags the two F_4TCNQ molecules toward each other until they are adjacent and better fill the π-stacked space. However, as we will show in Section 2.2.2, the free energy costs for inserting either one F_4TCNQ molecule or two F_4TCNQ molecules into the CTC geometry are similar, indicating that the critical nucleation size for creating the CTC polymorph is quite large. For this reason, we did not prepare systems with three or four F_4TCNQ molecules in the CTC polymorph.

2.1.4. Simulating the Fully F_4TCNQ Doped P3HT ICT and CTC Bulk Polymorphs. To simulate a fully doped F_4TCNQ:P3HT ICT polymorph, 288 negatively charged F_4TCNQ molecules were inserted into the lamellae of the simulated P3HT crystallites such that the dopant:monomer ratio was 1:6, which corresponds to a carrier density of 5.5×10^{20} cm^{-3}, similar to the experimentally measured carrier density at high doping levels: i.e., the doping level for the experimental structure factors in Figure 2.[59] For the corresponding positive charges, we placed 4 polarons on each of the 72 P3HT chains. The centers of the polarons were placed 6 monomer units apart, and on neighboring chains, the centers of the polarons were staggered by 3 monomer units, so that the polaron centers aligned with the dopant molecules as shown in Figure 3d. The 2σ value of the Gaussian polaronic charge distribution remained at 6 monomers, and where the polaronic charges on the same chain overlapped, the total charge on each thiophene unit was added. We did not consider the formation of bipolarons in our simulations, because

https://doi.org/10.1021/acsami.2c06449
ACS Appl. Mater. Interfaces 2022, 14, 26988−27001

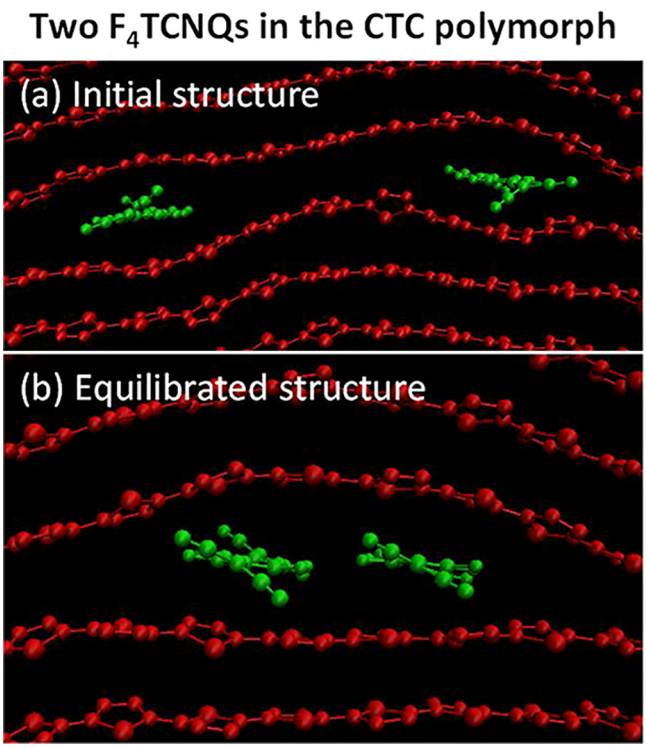

Figure 4. Snapshots of (a) the initial structure and (b) the structure after 10 ns equilibration of P3HT with two F_4TCNQ molecules inserted in the P3HT crystallite π-stacks (i.e., CTC polymorph) using the force field by Wildman et al.[50] Only a small fraction of the simulated cell is shown for clarity. The snapshots show the view looking down the hexyl chains (unit cell *a* axis, hexyl chains not shown), with the unit cell *b* axis running vertically. The atoms and bonds highlighted in red are part of the polymer backbone, and the F_4TCNQ molecules are highlighted in green. There is a free energy penalty to leave empty space in the polymer π-stacks between the dopant molecules, leading to a net force that drives the dopants to be adjacent in the π-stacked CTC polymorph.

bipolarons have never been experimentally observed when P3HT is doped with F_4TCNQ.

To simulate the case of the fully doped CTC polymorph, we inserted 144 F_4TCNQ molecules with a net charge of −0.59e (as with the single CTC case) into the simulated crystalline P3HT π-stacks: i.e., the dopant was incorporated at only a 1:12 dopant:monomer ratio rather than 1:6. We made this choice because, when we attempted to insert additional F_4TCNQ molecules, the doped P3HT no longer remained crystalline and did not show a well-defined polymorph, in contrast to the clear crystal to crystal transformation observed in experiments.[27] The positive countercharges for this case were treated in a manner similar to that for the fully doped ICT case, i.e., the delocalized polarons with +0.59e charge were placed 12 units apart and the delocalized polarons on neighboring chains were shifted by 6 units, to align with the dopant positions as depicted in Figure 3e.

2.1.5. Equilibration of the Different F_4TCNQ-Doped P3HT Systems. To ensure equilibration, all doped systems were annealed first at 400 K and then at 350 K for 1 ns each, after which they were equilibrated at room temperature for an additional 10 ns in the isobaric−isothermal ensemble (NPT). For all simulations except the fully doped CTC, we found that the polymorph crystal structure formed spontaneously during the final 10 ns equilibration step. For the fully doped CTC case, keeping a well-defined polymorph required a more complex equilibration process. This is because when we annealed the fully doped CTC system at higher temperatures starting from our manually generated initial configuration, many of the F_4TCNQ molecules moved from being π-stacked with the P3HT backbone to residing in the lamellae; in other words, we saw that heating caused the CTC polymorph to be converted into the ICT polymorph, as described in more detail in Section 2.3. We found that we could prevent the destruction of the CTC polymorph from happening if we equilibrated each of the six P3HT chain stacks separately, with the other stacks held fixed. Once each P3HT chain stack had been separately equilibrated, we then equilibrated the entire system at 300 K for an additional 10 ns. With this procedure, all but a few of the F_4TCNQ molecules remained π-stacked in the CTC polymorph.

2.1.6. Structure of Fully F_4TCNQ Doped P3HT Films. Having equilibrated the doped systems, we now examine the structures of the different polymorphs. As mentioned earlier, the Wildman et al. force field[50] does not do a good job of reproducing the unit cell tilt that takes place upon doping, but other force fields can capture this aspect (see Figure S2 in the Supporting Information). Figure 1c,d shows simulation snapshots of the fully doped ICT and CTC polymorphs for the P3HT chains, with the hexyl side chains not being shown for clarity. These panels show clearly that the F_4TCNQ molecules remain oriented with their long axes perpendicular to the P3HT backbone, essentially in the same orientation where we initially inserted them. This is consistent with experimental evidence studying rub-aligned films of F_4TCNQ-doped P3HT, which showed that the transition dipole for absorption of F_4TCNQ is entirely orthogonal to that of P3HT,[62] further indicating that the equilibrated doped structure simulation is in good agreement with experiment.

Experimentally, it is known that when P3HT is doped with F_4TCNQ in the ICT polymorph, the (100) peak shifts to a lower *q* value, while the (020) peak shifts to a higher *q* value.[63] This is because as F_4TCNQ molecules are inserted into the P3HT crystalline lamellae, the crystallites expand in the lamellar direction to accommodate the dopants, as visualized in Figure 1c. In fact, since P3HT chains lie edge-on to the substrate, the introduction of F_4TCNQ into P3HT films leads to an increase in film thickness of ∼15%,[64] about the size of the observed (100) lattice expansion. The decreased (020) spacing results from the change in the tilt of the P3HT unit cell *b* axis upon doping.

Figure 2b compares the simulated and experimental structure factors of undoped P3HT with the fully F_4TCNQ doped polymer in the ICT polymorph. The Wildman et al. force field[50] correctly reproduces the experimentally observed increase of the P3HT lamellar distance upon doping. In contrast, the force field does not correctly reproduce the experimental shift of the (020) peak to a higher *q* value, because it does not properly describe the tilt of the unit cell prior to ICT doping.

As far as we are aware, there are no experimental results available that describe the orientation or precise positions of the F_4TCNQ molecules in the CTC polymorph. Our simulations suggest that, as with the ICT polymorph, the long axis of the F_4TCNQ molecule prefers to orient perpendicularly to the P3HT backbone for the CTC polymorph (Figure 1d). Figure 1d also shows that in the fully doped CTC polymorph, the F_4TCNQ molecules tend to

https://doi.org/10.1021/acsami.2c06449
ACS Appl. Mater. Interfaces 2022, 14, 26988−27001

pair together, at least between different P3HT π-stacks. However, Figure 1d also suggests that there is less long-range order with the CTC polymorph than with the ICT polymorph, consistent with the fact that the CTC polymorph is harder to observe experimentally via X-ray diffraction.

For the structure factor of the fully doped CTC polymorph, shown in Figure 2b, with F_4TCNQ molecules located primarily in the P3HT π-stacks rather than in the lamellae, the calculations show a smaller shift of the (100) peak to a lower q value upon doping and essentially no shift of the (020) peak relative to the undoped material. Experimentally, we found in previous work that the CTC polymorph is characterized by a small shift to a higher q value of the ICT-phase lamellar (100) peak, though the CTC (100) peak is broad and overlaps the ICT peak, making a determination of precise peak positions difficult.[27] We also experimentally observed a shift of the π-stack (020) peak toward a higher q value as more CTCs were formed.[27] Thus, our simulations are in good qualitative but not quantitative agreement with experiment. The differences likely stem from the fact that the CTC state has more interdigitated side chains than either the neutral or the ICT states, but the Wildman et al. force field[50] does not produce significant interdigitation of the hexyl side chains in the CTC polymorph.

Overall, although the Wildman et al. force field[50] does not perfectly reproduce all of the experimentally observed details, it adequately describes the doped and undoped P3HT crystal structures. It appears to be better at capturing changes that occur in the P3HT lamellae in comparison to the tilting of the unit cell for the ICT polymorph. It accurately produces the experimental π-stack distance for the undoped polymer and gives good qualitative agreement for the structures of the fully doped polymer in both the ICT and CTC polymorphs.

2.2. Thermodynamics of Doping P3HT with F_4TCNQ in Different Polymorphs. With the nature of the force field and the simulation procedures for doping established, we now turn to using MD simulation to examine the thermodynamics of conjugated polymer doping. Our approach is to calculate the free energy cost of inserting F_4TCNQ molecules into P3HT crystallites using thermodynamic integration (TI), specifically the Bennett acceptance ratio method.[62,63] We only briefly discuss TI here, and details on how the calculations were carried out are given in the Supporting Information. Thermodynamic integration determines the free energy difference between two states by defining a thermodynamic path over a coordinate λ that connects the two states and then integrating the ensemble-averaged free energy change along that path. In our case, the two states are undoped P3HT and one of the F_4TCNQ-doped P3HT polymorphs, and the thermodynamic path is defined as first turning on the Lennard–Jones (LJ) interactions between the F_4TCNQ molecules and the P3HT chains (i.e., both the Lennard–Jones σ and ε parameters, referred to as λ_{LJ}) and then turning on the Coulomb interactions between them, labeled $\lambda_{Coulomb}$. Thus, our ($\lambda_{Coulomb}$,λ_{LJ}) TI coordinate starting point at (0,0) has no F_4TCNQ and the P3HT chains are undoped and electrically neutral. As λ_{LJ} is slowly increased over six to eight steps, the (0,1) state point corresponds to insertion of uncharged F_4TCNQ into the neutral P3HT lattice. Finally, as $\lambda_{Coulomb}$ is slowly increased over six steps, the (1,1) state point corresponds to having negatively charged F_4TCNQ and a delocalized polaron on the neighboring P3HT chains. At each intermediate point along the path, the system is equilibrated for 500 ps, and then an additional 500 ps trajectory is used to calculate the change in Gibbs free energy, ΔG. The change in enthalpy ΔH is then calculated with the built-in function of GROMACS using the positions of the atoms. Finally, the change in entropy ΔS is calculated using the definition of Gibbs free energy, $\Delta G \equiv \Delta H - T\Delta S$, with T = 300 K.

We choose this particular path treating the LJ and Coulomb interactions separately for two reasons. First, turning both interactions on simultaneously allowed the charges to become too close together at small values of the TI coordinate since there was insufficient repulsion between atoms to keep them apart; thus, the energy of the system could diverge. Second, examining the LJ and Coulomb terms separately also allows us to better understand the interplay of the two competing types of forces in the doping process. Turning on the LJ interactions describes the process of opening a hole in the P3HT crystal lattice to insert an F_4TCNQ molecule. This process is generally free energetically uphill, and we believe that this provides a reasonable approximation to the barrier for doping. Turning on the Coulomb interactions, on the other hand, is essentially the redox process that occurs upon doping, which stabilizes the system by generating an electron–hole pair or CTC. It is worth noting that all of the thermodynamic quantities we calculate are state functions that are path independent; thus, our conclusions do not depend on whether or not any particular part of our chosen path shows a barrier.

We note that our classical thermodynamic integration calculations do not include the quantum mechanical electrostatic energy change associated with charge transfer: i.e., the difference between the ionization energy of P3HT and the electron affinity of F_4TCNQ. The literature values for the HOMO of P3HT and the LUMO of F_4TCNQ are −5.0 and −5.24 eV, respectively, vs vacuum,[64−66] which gives chemical energy stabilizations of 240 and 142 meV (scaled by the 0.59e charge) per dopant for the ICT polymorph and the CTC polymorph, respectively. To account for this, we added this stabilization term, weighted by $\lambda_{Coulomb}$, to our calculations of $\Delta H_{Coulomb}$ in performing the thermodynamic integration.

Figure 5 shows the free-energy profile along our defined thermodynamic path, and Table 1 shows the calculated changes in free energy, enthalpy, and entropy for inserting F_4TCNQ into P3HT. Figure 5 and Table 1 explore three different systems: a single F_4TCNQ molecule inserted into the P3HT crystalline lamellae (blue squares, single ICT), a single F_4TCNQ molecule inserted between two π-stacked P3HT chains (orange circles, single CTC), and 288 F_4TCNQ molecules inserted into the lamellar region of the P3HT crystallites (yellow diamonds, fully doped ICT). The total free energies in Table 1 and Figure 5 include the enthalpic term due to the chemical energy difference of the P3HT valence band and the F_4TCNQ LUMO, described above, to better represent the total chemical driving force.

2.2.1. Thermodynamics of Inserting a Single F_4TCNQ Dopant into P3HT. We begin our exploration of the thermodynamics of conjugated polymer doping by studying what happens upon insertion of a single F_4TCNQ molecule either into the P3HT crystalline lamellae (single ICT) or between two π-stacked P3HT chains (single CTC). For the doping process, we see that when the dopant LJ interactions with the polymer are turned on, ΔH_{LJ}, ΔS_{LJ}, and ΔG_{LJ} are all more positive for insertion of a single F_4TCNQ into the CTC polymorph than for the ICT polymorph. The more positive

https://doi.org/10.1021/acsami.2c06449
ACS Appl. Mater. Interfaces 2022, 14, 26988−27001

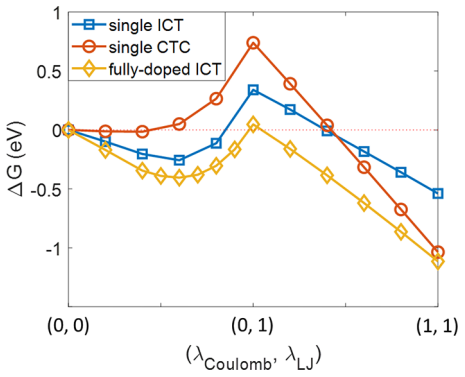

Figure 5. Free energy profile per dopant for insertion of F_4TCNQ into a P3HT crystallite along the thermodynamic integration path. The *x* axis is the thermodynamic integration coordinate, $(\lambda_{Coulomb},\lambda_{LJ})$. From (0,0) to (0,1), the LJ interactions are slowly turned on, and from (0,1) to (1,1), Coulomb interactions are slowly turned on. "single ICT" and "single CTC" show the profiles for inserting a single F_4TCNQ molecule into different locations (lamellae; π-stack) in the undoped P3HT crystallite, while "fully doped ICT" shows the profile for inserting 288 F_4TCNQ molecules into the P3HT crystalline lamellae (which we consider to be the "fully doped" state). The free energy profile for fully doped CTC is not shown, because no nucleation effect was observed for creating the CTC phase, as discussed in the text. The chemical energy change, multiplied by $\lambda_{Coulomb}$, is added to ΔG.

ΔH_{LJ} for CTC insertion reflects the larger enthalpic cost of creating space in the P3HT π-stacks in comparison to creating space in the P3HT lamellae. Creating space in the π-stacks involves bending the polymer backbone and significantly reorganizing the P3HT crystalline unit cell, whereas creating space in the P3HT lamellae only involves a modest rearrangement of the P3HT hexyl side chains and a tilting of the P3HT backbone.

Since ΔG_{LJ} approximately represents the barrier for doping, Figure 5 and Table 1 also suggest that the barrier for initially forming the CTC polymorph is higher than the barrier for inserting an F_4TCNQ molecule into the ICT polymorph. Thus, our simulations indicate that doping via ICT is more kinetically favored, which fits well with experiments which show that it is difficult to form the CTC polymorph.[12,26,27] However, even though the ICT polymorph is the more kinetically favored state, the total change in free energy, ΔG_{total}, is more negative for insertion of an F_4TCNQ into the CTC polymorph in comparison to the ICT polymorph. This indicates that, for insertion of a single dopant into undoped P3HT, the CTC polymorph is actually more thermodynamically favored, explaining why CTCs are always observed experimentally in doped P3HT films even if they are kinetically difficult to form.[27]

To verify that the thermodynamic quantities shown in Table 1 truly are path-independent, we also used TI to calculate the change in free energy for moving a F_4TCNQ dopant from the CTC configuration, π-stacked with the P3HT backbone, to the ICT configuration, among the P3HT side chains. The F_4TCNQ dopant in the initial CTC configuration and the F_4TCNQ dopant in the final ICT configuration are placed one P3HT stack apart (see Figure S7 in the Supporting Information). We connected the two states by simultaneously turning off the LJ and the Coulomb interactions for the F_4TCNQ dopant in the CTC configuration and turning on LJ and the Coulomb interactions for the F_4TCNQ dopant in the ICT configuration over 11 steps, as shown in Table S2 and Figure S8 in the Supporting Information. The TI-computed change in the free energy for converting a CTC dopant into an ICT dopant is indeed equal within error to the difference between the cost of inserting a dopant into the backbone and the cost of inserting a dopant into the lamellae. Thus, no matter how one traverses a thermodynamic cycle, the change in the free energy, which is a state function, depends only on the initial and the final structures and not the path.

The large barrier for dopant insertion suggests that the CTC phase forms more easily in amorphous regions of P3HT films, where there is less energetic cost to reordering the polymer π-stacks. This is also consistent with the experimental observation that the crystalline CTC polymorph only tends to form when the dopant is present in a solvent that can dissolve and thus completely restructure the P3HT crystallites[26,27] or when the P3HT side chains are engineered to block the dopants from being able to reside in the P3HT lamellae.[12]

2.2.2. Nucleating the Different F_4TCNQ-Doped P3HT Polymorphs. Having examined the thermodynamics for insertion of a single F_4TCNQ dopant into crystalline P3HT, we show in Figure 6 how $\Delta G_{Coulomb}$, ΔG_{LJ}, and ΔG_{total} per dopant change as the number of adjacently inserted F_4TCNQ molecules increases. The different geometries we chose for inserting neighboring F_4TCNQ molecules, shown in Figure 3

Table 1. ΔH, ΔS, and ΔG Values per Dopant for Insertion of F_4TCNQ into Different Locations in P3HT

		single ICT	fully doped ICT	single ICT
ΔH (eV)	LJ	0.610 ± 0.48	0.382 ± 0.003	2.90 ± 0.46
	Coulomb[a]	−0.855 ± 0.45	−1.27 ± 0.002	−4.28 ± 0.45
	total[a]	−0.245 ± 0.45	−0.888 ± 0.003	−1.38 ± 0.46
ΔS (meV K^{-1})	LJ	0.900 ± 1.6	1.12 ± 0.32	7.20 ± 1.5
	Coulomb	0.079 ± 1.5	−0.352 ± 0.21	−8.36 ± 1.5
	total	0.980 ± 1.5	0.764 ± 0.38	−1.16 ± 1.5
ΔG (eV)	LJ	0.340 ± 0.044	0.047 ± 0.096	0.739 ± 0.002
	Coulomb[a]	−0.878 ± 0.001	−1.16 ± 0.062	−1.78 ± 0.049
	total[a]	−0.538 ± 0.044	−1.12 ± 0.11	−1.04 ± 0.049

[a] $\Delta H_{Coulomb}$ and thus ΔH_{total}, $\Delta G_{Coulomb}$, and ΔG_{total} include an extra term due to chemical energy stabilization. The literature values for the HOMO of P3HT and the LUMO of F_4TCNQ are −5.0 and −5.24 eV, respectively, vs vacuum,[64−66] which gives chemical energy stabilizations of 240 and 142 meV (scaled by the 0.59e charge) for the ICT polymorph and the CTC polymorph, respectively.

https://doi.org/10.1021/acsami.2c06449
ACS Appl. Mater. Interfaces 2022, 14, 26988−27001

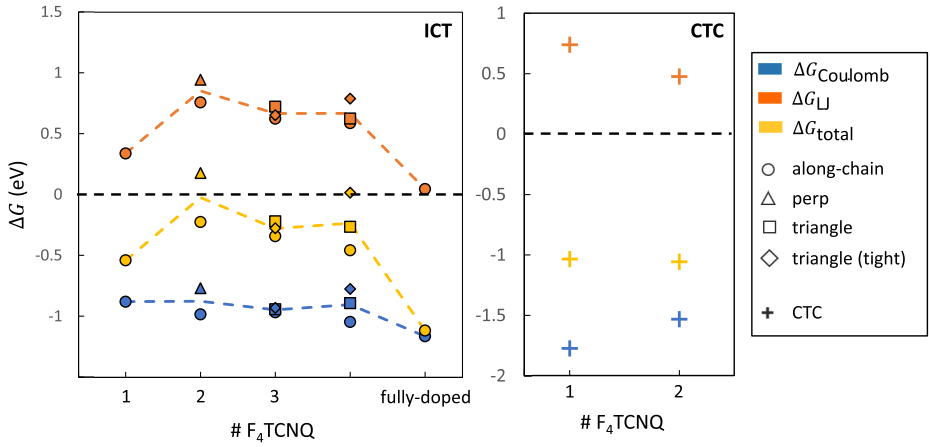

Figure 6. Change in free energy per dopant for inserting different numbers of F_4TCNQ molecules into undoped P3HT. ΔG_{LJ} (orange symbols) is the change in free energy for turning on the LJ interactions while the Coulomb interactions are kept off, i.e., going from $(\lambda_{Coulomb},\lambda_{LJ}) = (0, 0)$ to (0,1). $\Delta G_{Coulomb}$ is the change in free energy for turning on the Coulomb interactions while the LJ interactions are on: i.e., going from (0,1) to (1,1). ΔG_{total} (yellow symbols) is the overall change in free energy going from undoped to doped species. The different symbol shapes indicate different geometrical arrangements of placing the F_4TCNQ molecules in the P3HT crystalline lattice (see Figure 3). For the CTC polymorph, the polaron is only delocalized on a single chain. The dashed curves show the average free energy for insertion of F_4TCNQ in the different geometrical arrangements to help guide the eye. The chemical energy is included in $\Delta G_{Coulomb}$ and, thus, ΔG_{total}.

and discussed in Section 2.1.3, are represented by different symbols. Of the different arrangements that we explored, the "along-chain" geometry appears to have the lowest ΔG values per dopant. For the other three geometries, there does not appear to be a trend as to which arrangement is more stable. This suggests that, when additional F_4TCNQ molecules are inserted into the lamellar region, the F_4TCNQ molecules prefer to line up parallel to the polymer backbone: i.e., along the unit cell c axis. This finding, however, might be an artifact of the finite size of the simulation box. Since each P3HT chain has only 24 monomer units and the F_4TCNQ dopants are placed 6 monomer units apart, the maximum number of F_4TCNQ molecules for the "along-chain" orientation is only 4. Therefore, the "along-chain" orientation would reach the "fully-doped" limit sooner than the other orientations.

Regardless of how the F_4TCNQ molecules are arranged, the way the free energy changes with the number of inserted F_4TCNQ molecules in the ICT polymorph is roughly the same. For all neighboring geometries, ΔG_{total} per dopant increases from inserting one F_4TCNQ to inserting two F_4TCNQ molecules into the P3HT side-chain region and then decreases as additional F_4TCNQ molecules are inserted. This indicates a critical nucleation size of ~2 for forming the ICT polymorph. The subsequent decrease in ΔG_{total} with doping number is mainly driven by changes in ΔG_{LJ}: i.e. a lowering of the barrier for dopant insertion. Once a few F_4TCNQ molecules are inserted into the polymer lamellae, inserting additional F_4TCNQ molecules becomes easier because the lamellae have already started to expand and the P3HT unit cell has started to undergo its phase transition into the ICT polymorph. The very small critical nucleation size for the doping phase transition is consistent with experimental observations: X-ray diffraction experiments show that the (100) and (020) P3HT scattering peaks both shift as low levels of F_4TCNQ are added, showing a two-phase coexistence between doped and undoped polymorphs.[61] Once the material is fully converted to the doped polymorph, no further peak shifts are observed, even though significantly more F_4TCNQ dopant can be added to the polymer lattice before saturation is reached.[59]

It is also worth noting that, even though the dopants are all negatively charged, there appears to be no Coulomb free energy penalty for adding additional dopants in any of the geometries we considered. This is likely because the polaronic charges along the polymer chains that accompany the insertion of the first few dopants, along with the new polarons created by additional dopants, help to overcome any dopant−dopant and polaron−polaron repulsions (and our "fully doped" simulations are not in a doping concentration regime where bipolaron formation or other polaronic interactions are likely to be significant). Thus, the main driving force for creating the ICT polymorph is the reorganization of the P3HT unit cell. The tilting of the chain and the increasing of the lamellar spacing are effectively nucleated after only ~2 dopants are appropriately placed in the P3HT crystalline lattice.

In contrast, our simulations suggest that the creation of the CTC-doped polymorph does not show nucleation at these small sizes. The upper right panel of Figure 6 shows that the ΔG_{total} values per dopant for inserting one F_4TCNQ and inserting two adjacent F_4TCNQs into the P3HT π-stacks are basically the same, consistent with the presence of a significant barrier to forming this polymorph.

2.2.3. Thermodynamics of Forming Fully Doped F_4TCNQ:P3HT ICT and CTC Polymorphs. As mentioned in Section 2.1.5, in attempts to prepare the CTC polymorph, it was challenging to keep the F_4TCNQ molecules in the P3HT π-stacks, particularly at higher temperatures. Moreover, the fact that we saw no nucleation effects at a small size for producing the CTC-doped polymorph means either that the free energy cost for insertion per dopant for the fully doped polymorph is similar to that of a single F_4TCNQ in the CTC polymorph or that the critical domain size is very large. If we assume that the CTC insertion cost is independent of the number of dopants, then we can directly compare the free energy per dopant of the fully doped ICT polymorph to that of the CTC polymorph.

Table 1 shows that the fully doped ICT polymorph is entropically favored, while the CTC polymorph is enthalpically

https://doi.org/10.1021/acsami.2c06449
ACS Appl. Mater. Interfaces 2022, 14, 26988−27001

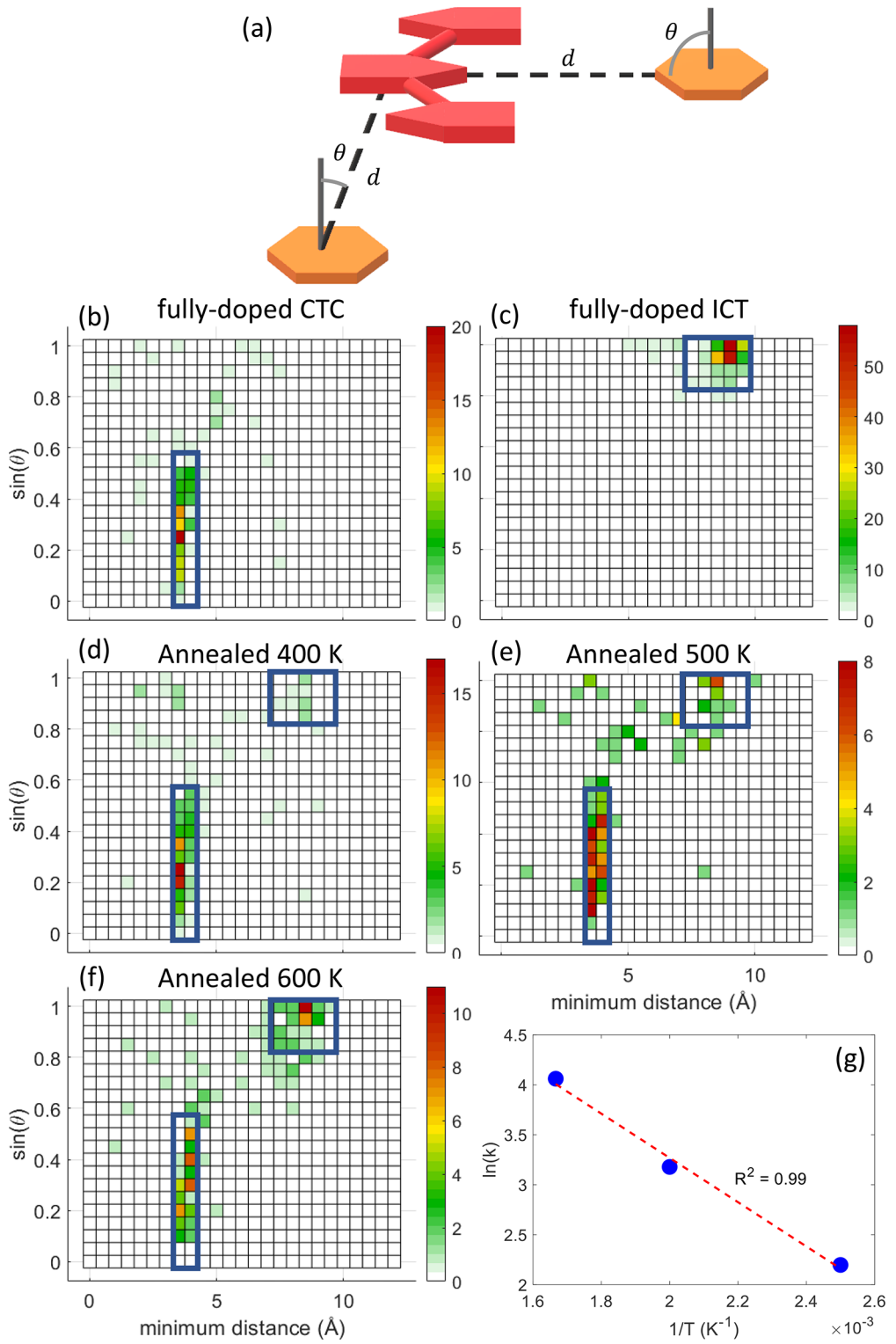

Figure 7. (a) Cartoon illustration of the coordinates used to define the location and the orientation of F_4TCNQ. The P3HT backbone is shown in red (the hexyl side chains are not shown), and F_4TCNQ is shown in orange (the cyano and fluoro groups are not shown). d is the distance between the centers of mass of F_4TCNQ and the closest P3HT thiophene ring. θ is the angle between the vector that connects the centers of mass and the normal vector of F_4TCNQ. The F_4TCNQ depicted below the P3HT chain shows the CTC polymorph, while the F_4TCNQ shown to the right of the P3HT chain is an example of the ICT polymorph. (b–f) Locations and orientations of F_4TCNQ molecules for fully doped CTC, fully doped ICT, and the fully doped CTC phase following thermal annealing at 400, 500, and 600 K, respectively. The bottom left blue rectangle highlights F_4TCNQ molecules that are π-stacking with the backbone (CTC polymorph). The upper right blue rectangle represents F_4TCNQ molecules that are sitting in the P3HT lamellae (ICT polymorph). (g) Arrhenius plot based on the number of CTC dopants that convert to the ICT phase at the different temperatures in (d–f).

https://doi.org/10.1021/acsami.2c06449
ACS Appl. Mater. Interfaces 2022, 14, 26988−27001

favored. For both fully doped polymorphs, there are three reasons we believe that the calculated entropy/enthalpy balance is qualitatively accurate. First, the CTC polymorph should have a lower (more negative) $\Delta H_{Coulomb}$ value in comparison to the ICT polymorph. Although the magnitude of the charges on the polymer and dopant are smaller for the CTC polymorph (±0.59e vs ±1e), the charges reside much more closely together in the CTC polymorph than in the ICT polymorph (~4 Å apart vs ~8 Å apart, respectively). Second, we expect the fully doped ICT polymorph to have a higher entropy than the CTC polymorph, because there are more ways to orient and distribute the F_4TCNQ molecules in the P3HT lamellae among the side chains than there are ways to π-stack the F_4TCNQ molecules with the polymer backbone. Finally and most importantly, experiments showed that thermally annealing doped films at only a slightly elevated temperature (80 °C for 5 min) caused the CTC polymorph to convert into the ICT polymorph.[27] This observation agrees with the calculated entropy/enthalpy balance of doping, which says that the ICT polymorph is entropically favored.

Overall, ΔG_{total} per dopant is roughly the same for the fully doped CTC and ICT polymorphs. The fully doped ICT polymorph is predicted to be more stable than the CTC polymorph, but only by ~79 meV. This is consistent with experiments which show that both the CTC and ICT polymorphs form simultaneously, even in the most crystalline films.[27] Moreover, the fact that the ICT polymorph is at most only slightly more stable than the CTC polymorph suggests that the relative amount of CTCs in doped films in experiments is determined more by the kinetics of the dopant infiltration method and not by thermodynamic stability.

2.3. Thermal Conversion of the CTC to the ICT Polymorph in F_4TCNQ-Doped P3HT. Because our chosen path for thermodynamic integration is arbitrary, to further explore the kinetics barriers involved in the formation of the CTC- and ICT-doped P3HT polymorphs, we simulated thermal annealing of the fully doped CTC polymorph at three different temperatures: 400, 500, and 600 K. With an equilibrated room-temperature configuration as the starting point, the system was annealed at each target temperature for 2 ns and then allowed to re-equilibrate at 300 K for an additional 6 ns. For this set of simulations, we held the values of the charges fixed at the CTC value of ±0.59e even if the dopant molecules moved from the P3HT π-stacks to the lamellae (i.e., converted from CTC to ICT). We note that this means that our simulations will underestimate the tendency for the CTC polymorph to convert to the ICT polymorph, since we are underestimating part of the Coulomb stabilization that would result with the ICT charge distribution.

Figure 7 summarizes the spatial reorganization of the F_4TCNQ molecules prior to and at the end of the simulated thermal annealing cycles. We use two parameters to characterize the location of the F_4TCNQ molecules in the P3HT crystallites, summarized in Figure 7a. The first parameter is the distance between the center of mass of the F_4TCNQ molecule and the center of mass of the closest thiophene unit, d. The second parameter is the sine of the angle θ between the normal vector of the F_4TCNQ molecule and the vector connecting the center of mass of the F_4TCNQ molecule and the center of mass of the nearest thiophene monomer. Figure 7 also shows the distributions of these parameters for the fully doped ICT (Figure 7c) and CTC (Figure 7b) polymorphs at room temperature.

With these definitions, we see that, for the equilibrium CTC polymorph (Figure 7b), the distribution of the distance d is fairly narrow at around 4 Å, reflecting the fact that the F_4TCNQ molecules are π-stacking with the neighboring thiophenes (light blue box at lower left). In contrast, the equilibrium ICT polymorph (Figure 7c) has a wider distribution of distances between the dopant and the thiophene backbone (light blue box at the upper right). The average d value of ~8 Å matches that observed in X-ray diffraction[59] and that predicted theoretically on the basis of IR spectroscopy of the polaron;[33] the width of the ICT polymorph d distribution reflects the large number of ways available for the dopant to sit in the crystalline lamellae. Figures 7b,c also shows that the distribution of sin θ is wider for the CTC polymorph than for the ICT polymorph. The fact that the CTC polymer:dopant π-stacks have a large degree of angular disorder (see also Figure 1d) may be one of the reasons it has been difficult to characterize the CTC polymorph experimentally.[26,27]

Figure 7d–f shows the change in the spatial distribution of F_4TCNQ dopants that results upon thermally annealing the fully doped room-temperature CTC polymorph at different temperatures. The results agree well with experiment in that our simulated annealing process shows a conversion of the CTC polymorph to the ICT polymorph.[27] On the basis of the thermodynamic data from the previous section, the entropic cost of forming the CTC polymorph is negative (unfavorable), whereas the entropic cost of forming the ICT polymorph is positive (favorable), and the difference in the entropic costs is ~2 meV K^{-1}. Therefore, modest changes in the temperature will significantly change the relative stabilities of the two phases. Figure 7f also shows that the CTCs which survived the annealing process at 600 K have an average sin θ value that is slightly smaller than that at 300 K, which means that only the CTCs where the F_4TCNQ and the nearby P3HT thiophene ring were almost parallel, i.e., the ones that were well π-stacked, are able to survive the annealing process.

If we define a molecule as being in the CTC or ITC polymorph if its d and sin θ parameters fall within the light blue boxes in Figure 7, we can determine precisely how many dopant molecules changed polymorph during the annealing process. Figure 7g plots the rate of CTC to ICT conversion based on the number of molecules that switched polymorphs as a function of the inverse temperature: i.e., an Arrhenius plot. The slope of the best-fit line provides an estimated activation barrier of ~140 meV for converting the CTC polymorph to the ICT polymorph. This simulated activation barrier is likely higher than the experimental value, particularly since we know experimentally that annealing at only 80 °C (~350 K) is enough to convert most of the CTC polymorph to the ICT polymorph.[27] One reason for the overestimation of the simulated barrier is the fact that we underestimate the Coulomb stabilization of the ICT phase in the annealing simulations, as mentioned above. In addition, the few nanoseconds of annealing time of these simulations is likely not enough time to reach population equilibrium, even at elevated temperatures. Overall, however, the simulations show clearly that the CTC polymorph has stability comparable to that of the ICT polymorph and that the application of modest thermal energy can convert many of the CTCs to the more desirable ICT phase.

https://doi.org/10.1021/acsami.2c06449
ACS Appl. Mater. Interfaces 2022, 14, 26988–27001

3. CONCLUSIONS

In this work, we simulated the F_4TCNQ doping of bulk P3HT in both the ICT and CTC polymorphs. The overall free energies to create the fully doped ICT and CTC polymorphs are similar, explaining why both phases always appear to be present experimentally. The barrier for insertion of a single F_4TCNQ molecule into P3HT, however, largely comes from the Lennard−Jones interactions between the dopant and the polymer, and we saw that the ΔG_{LJ} value is lower for the ICT phase than for the CTC phase. We also saw that ICT doping shows a nucleation effect: as more F_4TCNQ molecules are inserted into the P3HT lamellae, the lamellar region expands and the barrier for inserting additional dopants decreases. On the other hand, the CTC-doped polymorph does not show this behavior; thus, either it does not show nucleation effects or the critical nucleus size is very large. Either way, the different nucleation behaviors help explain why the CTC polymorph is experimentally harder to observe. Finally, our simulations indicated that the relative stability of the two polymorphs is highly temperature dependent: the entropic cost of making the CTC polymorph is negative, while it is positive for making the ICT polymorph. We also saw that by annealing the CTC polymorph at different temperatures, there was only a moderate activation barrier for converting the CTC polymorph to the ICT polymorph.

With the ICT polymorph and the CTC polymorph being roughly equally stable at room temperature, this means that, unfortunately, it will be nearly impossible to completely eliminate the undesirable CTC polymorph in F_4TCNQ-doped P3HT films. However, our simulations indicate that there are two ways to minimize the formation of the CTC polymorph. First, the simulations show that formation of the ICT polymorph is kinetically favored, which also explains the prevalence of the ICT phase experimentally. This means that we can minimize the creation of CTCs as long as the method chosen for dopant infiltration does not lower the barrier for placing dopants in the polymer π-stacks. Second, the simulations show that the formation of the ICT polymorph is entropically favored. This means that we can favor the ICT polymorph over the CTC polymorph with the application of modest annealing (i.e., at temperatures below that which causes dedoping of the polymer).

Overall, despite the use of classical mechanics and pre-existing force fields, our MD simulations paint a qualitatively accurate picture of the doping of P3HT with F_4TCNQ. With the insights learned about the relative stabilities, barriers for insertion, and nucleation effects, it should be possible to design a new generation of polymer:dopant systems to enhance the desired doped polymorph for a variety of applications.

4. SIMULATION METHODS

MD simulations and calculations were carried out using the GROMACS package.[53−56] DFT calculations were carried out using Gaussian[67] with PBE0-D3/6-31G(d,p). The parameters for the force field and the charges are given in the Supporting Information. All of the simulations were carried out with periodic boundary conditions in all three axes in the isothermal−isobaric (NPT) ensemble using the Berendsen thermostat with τ_p = 5.0 ps. The pressures is set to match the experimental density of pure P3HT films. A time step of 1 fs and a leapfrog integration algorithm were used. Electrostatics were treated using the fast smooth particle-mesh Ewald (SPME) with a cutoff at 1.4 nm, a Fourier spacing of 0.12 nm, and a PME order of 4. The van der Waals cutoff was set at 1.4 nm. For thermodynamic integration, a soft function with σ = 0.3 and α = 0.5 is used for λ. An example mdp file, which sets all the MD parameters used in one of the TI calculations can be found at the end of the Supporting Information.

■ ASSOCIATED CONTENT

Supporting Information

The Supporting Information is available free of charge at https://pubs.acs.org/doi/10.1021/acsami.2c06449.

Results from several other force fields to show that our conclusions are qualitatively robust, force field parameters, and GIWAXS experiments (PDF)

■ AUTHOR INFORMATION

Corresponding Author

Benjamin J. Schwartz − *Department of Chemistry and Biochemistry, University of California, Los Angeles, Los Angeles, California 90095-1569, United States;* orcid.org/0000-0003-3257-9152; Email: schwartz@chem.ucla.edu

Authors

Eric Chih-Kuan Wu − *Department of Chemistry and Biochemistry, University of California, Los Angeles, Los Angeles, California 90095-1569, United States*

Charlene Z. Salamat − *Department of Chemistry and Biochemistry, University of California, Los Angeles, Los Angeles, California 90095-1569, United States*

Sarah H. Tolbert − *Departments of Chemistry and Biochemistry and Materials Science and Engineering, University of California, Los Angeles, Los Angeles, California 90095-1569, United States;* orcid.org/0000-0001-9969-1582

Complete contact information is available at: https://pubs.acs.org/10.1021/acsami.2c06449

Notes

The authors declare no competing financial interest.

■ ACKNOWLEDGMENTS

We gratefully acknowledge the support of funding from the National Science Foundation through grant numbers CHE-2003755 and DMR-2105896. Computations were performed on the Hoffman 2 cluster operated by the UCLA Institute for Digital Research and Education. This research used resources of the Advanced Photon Source, a U.S. Department of Energy (DOE) Office of Science User Facility, operated for the DOE Office of Science by Argonne National Laboratory under Contract No. DE-AC02-06CH11357.

■ REFERENCES

(1) Kuik, M.; Wetzelaer, G.-J. A. H.; Nicolai, H. T.; Craciun, N. I.; de Leeuw, D. M.; Blom, P. W. M. 25th Anniversary Article: Charge Transport and Recombination in Polymer Light-Emitting Diodes. *Adv. Mater.* **2014**, *26* (4), 512−531.

(2) Dou, L.; You, J.; Hong, Z.; Xu, Z.; Li, G.; Street, R. A.; Yang, Y. 25th Anniversary Article: A Decade of Organic/Polymeric Photovoltaic Research. *Adv. Mater.* **2013**, *25* (46), 6642−6671.

(3) Russ, B.; Glaudell, A.; Urban, J. J.; Chabinyc, M. L.; Segalman, R. A. Organic Thermoelectric Materials for Energy Harvesting and Temperature Control. *Nat. Rev. Mater.* **2016**, *1* (10), 16050.

(4) Cowart, J. S.; Liman, C.; Garnica, A.; Page, Z. A.; Lim, E.; Zope, R. R.; Baruah, T.; Hawker, C. J.; Chabinyc, M. L. Donor-Fullerene Dyads for Energy Cascade Organic Solar Cells. *Inorg. Chim. Acta* **2017**, *468*, 192−202.

(5) Hou, L.; Zhang, X.; Cotella, G. F.; Carnicella, G.; Herder, M.; Schmidt, B. M.; Pätzel, M.; Hecht, S.; Cacialli, F.; Samorì, P. Optically

Switchable Organic Light-Emitting Transistors. *Nat. Nanotechnol.* **2019**, *14* (4), 347−353.
(6) Bryan, C. D.; Cordes, A. W.; Fleming, R. M.; George, N. A.; Glarum, S. H.; Haddon, R. C.; Oakley, R. T.; Palstra, T. T. M.; Perel, A. S.; Schneemeyer, L. F.; Waszczak, J. v. Conducting Charge-Transfer Salts Based on Neutral π-Radicals. *Nature* **1993**, *365* (6449), 821−823.
(7) Goetz, K. P.; Vermeulen, D.; Payne, M. E.; Kloc, C.; McNeil, L. E.; Jurchescu, O. D. Charge-Transfer Complexes: New Perspectives on an Old Class of Compounds. *J. Mater. Chem. C* **2014**, *2* (17), 3065−3076.
(8) Torrance, J. B.; Silverman, B. D. Charge Transfer and Ionic Bonding in Organic Solids with Segregated Stacks. *Phys. Rev. B* **1977**, *15* (2), 788−801.
(9) Ferraris, J.; Cowan, D. O.; Walatka, V.; Perlstein, J. H. Electron Transfer in a New Highly Conducting Donor-Acceptor Complex. *J. Am. Chem. Soc.* **1973**, *95* (3), 948−949.
(10) Torrance, J. B.; Scott, B. A.; Kaufman, F. B. Optical Properties of Charge Transfer Salts of Tetracyanoquinodimethane (TCNQ). *Solid State Commun.* **1993**, *88* (11−12), 971−975.
(11) Ghani, F.; Opitz, A.; Pingel, P.; Heimel, G.; Salzmann, I.; Frisch, J.; Neher, D.; Tsami, A.; Scherf, U.; Koch, N. Charge Transfer in and Conductivity of Molecularly Doped Thiophene-Based Copolymers. *J. Polym. Sci., Part B: Polym. Phys.* **2015**, *53* (1), 58−63.
(12) Thomas, E. M.; Davidson, E. C.; Katsumata, R.; Segalman, R. A.; Chabinyc, M. L. Branched Side Chains Govern Counterion Position and Doping Mechanism in Conjugated Polythiophenes. *ACS Macro Lett.* **2018**, *7* (12), 1492−1497.
(13) Kang, K.; Watanabe, S.; Broch, K.; Sepe, A.; Brown, A.; Nasrallah, I.; Nikolka, M.; Fei, Z.; Heeney, M.; Matsumoto, D.; Marumoto, K.; Tanaka, H.; Kuroda, S.; Sirringhaus, H. 2D Coherent Charge Transport in Highly Ordered Conducting Polymers Doped by Solid State Diffusion. *Nat. Mater.* **2016**, *15* (8), 896−902.
(14) Hamidi-Sakr, A.; Biniek, L.; Bantignies, J.-L.; Maurin, D.; Herrmann, L.; Leclerc, N.; Lévêque, P.; Vijayakumar, V.; Zimmermann, N.; Brinkmann, M. A Versatile Method to Fabricate Highly In-Plane Aligned Conducting Polymer Films with Anisotropic Charge Transport and Thermoelectric Properties: The Key Role of Alkyl Side Chain Layers on the Doping Mechanism. *Adv. Funct. Mater.* **2017**, *27* (25), 1700173.
(15) Aubry, T. J.; Axtell, J. C.; Basile, V. M.; Winchell, K. J.; Lindemuth, J. R.; Porter, T. M.; Liu, J.; Alexandrova, A. N.; Kubiak, C. P.; Tolbert, S. H.; Spokoyny, A. M.; Schwartz, B. J. Dodecaborane-Based Dopants Designed to Shield Anion Electrostatics Lead to Increased Carrier Mobility in a Doped Conjugated Polymer. *Adv. Mater.* **2019**, *31* (11), 1805647.
(16) Salzmann, I.; Heimel, G. Toward a Comprehensive Understanding of Molecular Doping Organic Semiconductors (Review). *J. Electron Spectrosc. Relat. Phenom.* **2015**, *204*, 208−222.
(17) Scholes, D. T.; Hawks, S. A.; Yee, P. Y.; Wu, H.; Lindemuth, J. R.; Tolbert, S. H.; Schwartz, B. J. Overcoming Film Quality Issues for Conjugated Polymers Doped with F_4TCNQ by Solution Sequential Processing: Hall Effect, Structural, and Optical Measurements. *J. Phys. Chem. Lett.* **2015**, *6* (23), 4786−4793.
(18) Fuzell, J.; Jacobs, I. E.; Ackling, S.; Harrelson, T. F.; Huang, D. M.; Larsen, D.; Moulé, A. J. Optical Dedoping Mechanism for P3HT:F_4TCNQ Mixtures. *J. Phys. Chem. Lett.* **2016**, *7* (21), 4297−4303.
(19) Jacobs, I. E.; Aasen, E. W.; Oliveira, J. L.; Fonseca, T. N.; Roehling, J. D.; Li, J.; Zhang, G.; Augustine, M. P.; Mascal, M.; Moulé, A. J. Comparison of Solution-Mixed and Sequentially Processed P3HT:F_4TCNQ Films: Effect of Doping-Induced Aggregation on Film Morphology. *J. Mater. Chem. C* **2016**, *4* (16), 3454−3466.
(20) Neelamraju, B.; Watts, K. E.; Pemberton, J. E.; Ratcliff, E. L. Correlation of Coexistent Charge Transfer States in F_4TCNQ-Doped P3HT with Microstructure. *J. Phys. Chem. Lett.* **2018**, *9* (23), 6871−6877.
(21) Watts, K. E.; Neelamraju, B.; Ratcliff, E. L.; Pemberton, J. E. Stability of Charge Transfer States in F_4TCNQ-Doped P3HT. *Chem. Mater.* **2019**, *31* (17), 6986−6994.
(22) Pingel, P.; Neher, D. Comprehensive Picture of p-Type Doping of P3HT with the Molecular Acceptor F_4TCNQ. *Phys. Rev. B* **2013**, *87* (11), 115209.
(23) Zapata-Arteaga, O.; Dörling, B.; Perevedentsev, A.; Martín, J.; Reparaz, J. S.; Campoy-Quiles, M. Closing the Stability−Performance Gap in Organic Thermoelectrics by Adjusting the Partial to Integer Charge Transfer Ratio. *Macromolecules* **2020**, *53* (2), 609−620.
(24) Jacobs, I. E.; Cendra, C.; Harrelson, T. F.; Bedolla Valdez, Z. I.; Faller, R.; Salleo, A.; Moulé, A. J. Polymorphism Controls the Degree of Charge Transfer in a Molecularly Doped Semiconducting Polymer. *Mater. Horiz.* **2018**, *5* (4), 655−660.
(25) Scholes, D. T.; Yee, P. Y.; Lindemuth, J. R.; Kang, H.; Onorato, J.; Ghosh, R.; Luscombe, C. K.; Spano, F. C.; Tolbert, S. H.; Schwartz, B. J. The Effects of Crystallinity on Charge Transport and the Structure of Sequentially Processed F_4TCNQ-Doped Conjugated Polymer Films. *Adv. Funct. Mater.* **2017**, *27* (44), 1702654.
(26) Aubry, T. J.; Winchell, K. J.; Salamat, C. Z.; Basile, V. M.; Lindemuth, J. R.; Stauber, J. M.; Axtell, J. C.; Kubena, R. M.; Phan, M. D.; Bird, M. J.; Spokoyny, A. M.; Tolbert, S. H.; Schwartz, B. J. Tunable Dopants with Intrinsic Counterion Separation Reveal the Effects of Electron Affinity on Dopant Intercalation and Free Carrier Production in Sequentially Doped Conjugated Polymer Films. *Adv. Funct. Mater.* **2020**, *30* (28), 2001800.
(27) Stanfield, D. A.; Wu, Y.; Tolbert, S. H.; Schwartz, B. J. Controlling the Formation of Charge Transfer Complexes in Chemically Doped Semiconducting Polymers. *Chem. Mater.* **2021**, *33* (7), 2343−2356.
(28) Mombrú, D.; Romero, M.; Faccio, R.; Mombrú, Á. W. Unraveling the Lithium Bis(Trifluoromethanesulfonyl)Imide (LiTFSI) Doping Mechanism of Regioregular Poly(3-Hexylthiophene): Experimental and Theoretical Study. *J. Phys. Chem. C* **2020**, *124* (13), 7061−7070.
(29) Salzmann, I.; Heimel, G.; Oehzelt, M.; Winkler, S.; Koch, N. Molecular Electrical Doping of Organic Semiconductors: Fundamental Mechanisms and Emerging Dopant Design Rules. *Acc. Chem. Res.* **2016**, *49* (3), 370−378.
(30) Valencia, A. M.; Cocchi, C. Electronic and Optical Properties of Oligothiophene-F_4TCNQ Charge-Transfer Complexes: The Role of the Donor Conjugation Length. *J. Phys. Chem. C* **2019**, *123* (14), 9617−9623.
(31) Thomas, A. K.; Datko, B. D.; Grey, J. K. Charge Transfer Doping of Conjugated Polymers with Large Vibrational Activities: Insights into the Regime of Partial Charge Transfer. *J. Phys. Chem. C* **2020**, *124* (3), 2137−2145.
(32) Méndez, H.; Heimel, G.; Winkler, S.; Frisch, J.; Opitz, A.; Sauer, K.; Wegner, B.; Oehzelt, M.; Röthel, C.; Duhm, S.; Többens, D.; Koch, N.; Salzmann, I. Charge-Transfer Crystallites as Molecular Electrical Dopants. *Nat. Commun.* **2015**, *6* (1), 8560.
(33) Ghosh, R.; Pochas, C. M.; Spano, F. C. Polaron Delocalization in Conjugated Polymer Films. *J. Phys. Chem. C* **2016**, *120* (21), 11394−11406.
(34) Schwermann, C.; Doltsinis, N. L. Exciton Transfer Free Energy from Car−Parrinello Molecular Dynamics. *Phys. Chem. Chem. Phys.* **2020**, *22* (19), 10526−10535.
(35) Poelking, C.; Daoulas, K.; Troisi, A.; Andrienko, D. Morphology and Charge Transport in P3HT: A Theorist's Perspective. In *P3HT Revisited − From Molecular Scale to Solar Cell Devices*, Ludwigs, S. Ed.; Springer: 2014; Advances in Polymer Science, Vol. *265*, pp139−180. DOI: 10.1007/12_2014_277.
(36) Alexiadis, O.; Mavrantzas, V. G. All-Atom Molecular Dynamics Simulation of Temperature Effects on the Structural, Thermodynamic, and Packing Properties of the Pure Amorphous and Pure Crystalline Phases of Regioregular P3HT. *Macromolecules* **2013**, *46* (6), 2450−2467.

(37) Do, K.; Huang, D. M.; Faller, R.; Moulé, A. J. A Comparative MD Study of the Local Structure of Polymer Semiconductors P3HT and PBTTT. *Phys. Chem. Chem. Phys.* **2010**, *12* (44), 14735.
(38) Cheung, D. L.; McMahon, D. P.; Troisi, A. Computational Study of the Structure and Charge-Transfer Parameters in Low-Molecular-Mass P3HT. *J. Phys. Chem. B* **2009**, *113* (28), 9393−9401.
(39) Dag, S.; Wang, L.-W. Packing Structure of Poly(3-Hexylthiophene) Crystal: Ab Initio and Molecular Dynamics Studies. *J. Phys. Chem. B* **2010**, *114* (18), 5997−6000.
(40) Zhugayevych, A.; Mazaleva, O.; Naumov, A.; Tretiak, S. Lowest-Energy Crystalline Polymorphs of P3HT. *J. Phys. Chem. C* **2018**, *122* (16), 9141−9151.
(41) Borzdun, N. I.; Larin, S. v.; Falkovich, S. G.; Nazarychev, V. M.; Volgin, I. v.; Yakimansky, A. v.; Lyulin, A. v.; Negi, V.; Bobbert, P. A.; Lyulin, S. v. Molecular Dynamics Simulation of Poly(3-Hexylthiophene) Helical Structure In Vacuo and in Amorphous Polymer Surrounding. *J. Polym. Sci., Part B: Polym. Phys.* **2016**, *54* (23), 2448−2456.
(42) Root, S. E.; Savagatrup, S.; Pais, C. J.; Arya, G.; Lipomi, D. J. Predicting the Mechanical Properties of Organic Semiconductors Using Coarse-Grained Molecular Dynamics Simulations. *Macromolecules* **2016**, *49* (7), 2886−2894.
(43) Alberga, D.; Mangiatordi, G. F.; Torsi, L.; Lattanzi, G. Effects of Annealing and Residual Solvents on Amorphous P3HT and PBTTT Films. *J. Phys. Chem. C* **2014**, *118* (16), 8641−8655.
(44) Alberga, D.; Perrier, A.; Ciofini, I.; Mangiatordi, G. F.; Lattanzi, G.; Adamo, C. Morphological and Charge Transport Properties of Amorphous and Crystalline P3HT and PBTTT: Insights from Theory. *Phys. Chem. Chem. Phys.* **2015**, *17* (28), 18742−18750.
(45) Gross, J.; Ivanov, M.; Janke, W. Comparing Atomistic and Coarse-Grained Simulations of P3HT. *J. Phys.: Conf. Ser.* **2016**, *750*, 012009.
(46) Tummala, N. R.; Risko, C.; Bruner, C.; Dauskardt, R. H.; Brédas, J.-L. Entanglements in P3HT and Their Influence on Thin-Film Mechanical Properties: Insights from Molecular Dynamics Simulations. *J. Polym. Sci., Part B: Polym. Phys.* **2015**, *53* (13), 934−942.
(47) Tsourtou, F. D.; Peristeras, L. D.; Apostolov, R.; Mavrantzas, V. G. Molecular Dynamics Simulation of Amorphous Poly(3-Hexylthiophene). *Macromolecules* **2020**, *53* (18), 7810−7824.
(48) Wolf, C. M.; Kanekal, K. H.; Yimer, Y. Y.; Tyagi, M.; Omar-Diallo, S.; Pakhnyuk, V.; Luscombe, C. K.; Pfaendtner, J.; Pozzo, L. D. Assessment of Molecular Dynamics Simulations for Amorphous Poly(3-Hexylthiophene) Using Neutron and X-Ray Scattering Experiments. *Soft Matter* **2019**, *15* (25), 5067−5083.
(49) Jorgensen, W. L.; Maxwell, D. S.; Tirado-Rives, J. Development and Testing of the OPLS All-Atom Force Field on Conformational Energetics and Properties of Organic Liquids. *J. Am. Chem. Soc.* **1996**, *118* (45), 11225−11236.
(50) Wildman, J.; Repiščák, P.; Paterson, M. J.; Galbraith, I. General Force-Field Parametrization Scheme for Molecular Dynamics Simulations of Conjugated Materials in Solution. *J. Chem. Theory Comput.* **2016**, *12* (8), 3813−3824.
(51) Prentice, A. W.; Wildman, J.; Galbraith, I.; Paterson, M. J. Properties of Conjugated Materials from Quantum Chemistry Coupled to Molecular Dynamics Generated Ensembles. *J. Phys. Chem. A* **2020**, *124* (51), 10667−10677.
(52) Hanwell, M. D.; Curtis, D. E.; Lonie, D. C.; Vandermeersch, T.; Zurek, E.; Hutchison, G. R. Avogadro: An Advanced Semantic Chemical Editor, Visualization, and Analysis Platform. *J. Cheminf.* **2012**, *4* (1), 17.
(53) van der Spoel, D.; Lindahl, E.; Hess, B.; Groenhof, G.; Mark, A. E.; Berendsen, H. J. C. GROMACS: Fast, Flexible, and Free. *J. Comput. Chem.* **2005**, *26* (16), 1701−1718.
(54) Lindahl, E.; Hess, B.; van der Spoel, D. GROMACS 3.0: A Package for Molecular Simulation and Trajectory Analysis. *J. Mol. Model.* **2001**, *7*, 306−317.
(55) Hess, B.; Kutzner, C.; van der Spoel, D.; Lindahl, E. GROMACS 4: Algorithms for Highly Efficient, Load-Balanced, and Scalable Molecular Simulation. *J. Chem. Theory Comput.* **2008**, *4* (3), 435−447.
(56) Pronk, S.; Pall, S.; Schulz, R.; Larsson, P.; Bjelkmar, P.; Apostolov, R.; Shirts, M. R.; Smith, J. C.; Kasson, P. M.; van der Spoel, D.; Hess, B.; Lindahl, E. GROMACS 4.5: A High-Throughput and Highly Parallel Open Source Molecular Simulation Toolkit. *Bioinformatics* **2013**, *29* (7), 845−854.
(57) Kayunkid, N.; Uttiya, S.; Brinkmann, M. Structural Model of Regioregular Poly(3-Hexylthiophene) Obtained by Electron Diffraction Analysis. *Macromolecules* **2010**, *43* (11), 4961−4967.
(58) Yee, P. Y.; Scholes, D. T.; Schwartz, B. J.; Tolbert, S. H. Dopant-Induced Ordering of Amorphous Regions in Regiorandom P3HT. *J. Phys. Chem. Lett.* **2019**, *10* (17), 4929−4934.
(59) Hamidi-Sakr, A.; Biniek, L.; Fall, S.; Brinkmann, M. Precise Control of Lamellar Thickness in Highly Oriented Regioregular Poly(3-Hexylthiophene) Thin Films Prepared by High-Temperature Rubbing: Correlations with Optical Properties and Charge Transport. *Adv. Funct. Mater.* **2016**, *26* (3), 408−420.
(60) Stanfield, D. A.; Mehmedović, Z.; Schwartz, B. J. Vibrational Stark Effect Mapping of Polaron Delocalization in Chemically Doped Conjugated Polymers. *Chem. Mater.* **2021**, *33* (21), 8489−8500.
(61) Untilova, V.; Biskup, T.; Biniek, L.; Vijayakumar, V.; Brinkmann, M. Control of Chain Alignment and Crystallization Helps Enhance Charge Conductivities and Thermoelectric Power Factors in Sequentially Doped P3HT:F_4TCNQ Films. *Macromolecules* **2020**, *53* (7), 2441−2453.
(62) Bennett, C. H. Efficient Estimation of Free Energy Differences from Monte Carlo Data. *J. Comput. Phys.* **1976**, *22* (2), 245−268.
(63) Wu, D.; Kofke, D. A. Phase-Space Overlap Measures. II. Design and Implementation of Staging Methods for Free-Energy Calculations. *J. Chem. Phys.* **2005**, *123* (8), 084109.
(64) Gao, W.; Kahn, A. Controlled p -Doping of Zinc Phthalocyanine by Coevaporation with Tetrafluorotetracyanoquinodimethane: A Direct and Inverse Photoemission Study. *Appl. Phys. Lett.* **2001**, *79* (24), 4040−4042.
(65) Kivala, M.; Boudon, C.; Gisselbrecht, J.-P.; Enko, B.; Seiler, P.; Müller, I. B.; Langer, N.; Jarowski, P. D.; Gescheidt, G.; Diederich, F. Organic Super-Acceptors with Efficient Intramolecular Charge-Transfer Interactions by [2 + 2] Cycloadditions of TCNE, TCNQ, and F_4TCNQ to Donor-Substituted Cyanoalkynes. *Chem. - Eur. J.* **2009**, *15* (16), 4111−4123.
(66) Jacobs, I. E.; Moulé, A. J. Controlling Molecular Doping in Organic Semiconductors. *Adv. Mater.* **2017**, *29* (42), 1703063.
(67) *Gaussian 09, Rev. A.02*; Gaussian, Inc.: 2016. https://www.gaussian.com.

https://doi.org/10.1021/acsami.2c06449
ACS Appl. Mater. Interfaces 2022, 14, 26988−27001